Molecular Neurobiology (2019) 56:3638–3656
https://doi.org/10.1007/s12035-018-1333-0

Pantothenate Rescues Iron Accumulation in Pantothenate Kinase-Associated Neurodegeneration Depending on the Type of Mutation

Mónica Álvarez-Córdoba[1,2] · Aida Fernández Khoury[1,2] · Marina Villanueva-Paz[1,2] · Carmen Gómez-Navarro[1,2] · Irene Villalón-García[1,2] · Juan M. Suárez-Rivero[1,2] · Suleva Povea-Cabello[1,2] · Mario de la Mata[1,2] · David Cotán[1,2] · Marta Talaverón-Rey[1,2] · Antonio J. Pérez-Pulido[3] · Joaquín J. Salas[4] · Eva Mª Pérez-Villegas[5] · Antonio Díaz-Quintana[6] · José A. Armengol[5] · José A. Sánchez-Alcázar[1,2]

Received: 28 February 2018 / Accepted: 24 August 2018 / Published online: 1 September 2018

Abstract

Neurodegeneration with brain iron accumulation (NBIA) is a group of inherited neurologic disorders in which iron accumulates in the basal ganglia resulting in progressive dystonia, spasticity, parkinsonism, neuropsychiatric abnormalities, and optic atrophy or retinal degeneration. The most prevalent form of NBIA is pantothenate kinase-associated neurodegeneration (PKAN) associated with mutations in the gene of pantothenate kinase 2 (PANK2), which is essential for coenzyme A (CoA) synthesis. There is no cure for NBIA nor is there a standard course of treatment. In the current work, we describe that fibroblasts derived from patients harbouring PANK2 mutations can reproduce many of the cellular pathological alterations found in the disease, such as intracellular iron and lipofuscin accumulation, increased oxidative stress, and mitochondrial dysfunction. Furthermore, mutant fibroblasts showed a characteristic senescent morphology. Treatment with pantothenate, the PANK2 enzyme substrate, was able to correct all pathological alterations in responder mutant fibroblasts with residual PANK2 enzyme expression. However, pantothenate had no effect on mutant fibroblasts with truncated/incomplete protein expression. The positive effect of pantothenate in particular mutations was also confirmed in induced neurons obtained by direct reprograming of mutant fibroblasts. Our results suggest that pantothenate treatment can stabilize the expression levels of PANK2 in selected mutations. These results encourage us to propose our screening model as a quick and easy way to detect pantothenate-responder patients with PANK2 mutations. The existence of residual enzyme expression in some affected individuals raises the possibility of treatment using high dose of pantothenate.

Keywords Pantothenate kinase · Coenzyme A · Mitochondria · Pantothenate · Induced neurons

Introduction

Neurodegeneration with brain iron accumulation (NBIA) is a group of rare neurodegenerative disorders characterized by progressive extrapyramidal dysfunction (dystonia, rigidity, choreoathetosis), iron accumulation in the brain, and the presence of axonal spheroids, corresponding to degenerating neurons, usually limited to the central nervous system [1, 2].

Electronic supplementary material The online version of this article (https://doi.org/10.1007/s12035-018-1333-0) contains supplementary material, which is available to authorized users.

✉ José A. Sánchez-Alcázar
jasanalc@upo.es; http://www.upo.es/CABD/

[1] Centro Andaluz de Biología del Desarrollo (CABD-CSIC), Universidad Pablo de Olavide, Carretera de Utrera Km 1, 41013 Sevilla, Spain

[2] Centro de Investigación Biomédica en Red: Enfermedades Raras, Instituto de Salud Carlos III, Carretera de Utrera Km 1, 41013 Sevilla, Spain

[3] Departamento de Biología Molecular e Ingeniería Bioquímica, Universidad Pablo de Olavide, Sevilla, Spain

[4] Departamento de Bioquímica y Biología Molecular de Productos Vegetales, Instituto de la Grasa (CSIC), Sevilla, Spain

[5] Departamento de Fisiología, Anatomía y Biología Celular, Universidad Pablo de Olavide, 41013 Sevilla, Spain

[6] Instituto de Investigaciones Químicas (IIQ)—Centro de Investigaciones Científicas Isla de la Cartuja (cicCartuja), Universidad de Sevilla—CSIC, Sevilla, Spain

Several causative genes underlying NBIA have been identified which explain about 65% of cases. By now, 12 established genes, with their causative mutations, are known to cause different subtypes of NBIA [3]. However, around 20% of cases are still genetically undefined [4].

The most common form of NBIA is pantothenate kinase-associated neurodegeneration (PKAN) which is associated with a defect in the gene of pantothenate kinase 2 (PANK2), which encodes an essential enzyme in coenzyme A (CoA) synthesis; it represents approximately 50% of cases [5]. The pantothenate kinase gene family includes PANK1a, PANK1b, PANK2, and PANK3, but only PANK2 is the causative gene for NBIA. PANK2 transforms (R)-pantothenate into (R)-4′-phosphopantothenate using ATP; it is regulated by feedback inhibition by CoA and its thioesters. Pantothenate or vitamin B5 is the main precursor for the synthesis of CoA. The enzyme deficiency causes an insufficient energy production, biosynthesis alterations at cell membrane replacement, and loss of protection against oxidative damage provided by CoA and glutathione peroxidase/glutathione reductase system. Reactive oxygen species (ROS) accumulation increases due to deposits of iron and cysteine, which increase the susceptibility of suffer harmful effects at some cell regions and can induce lipid peroxidation, which can cause membrane damage and activate apoptosis. PANK2-defective neurons derived from KO mice have an altered mitochondrial membrane potential and defective mitochondrial respiration [6].

However, the exact etiology of PKAN is not known. One proposed hypothesis is that abnormal peroxidation of lipofuscin to neuromelanin and deficient cysteine dioxygenase lead to abnormal iron accumulation in the brain [7]. PKAN is a devastating disorder for which only symptomatic treatments are currently available.

Attempts to generate animal models of the disease have produced incomplete phenotypes, possibly because the mitochondrial localization of PANK2 has only been reported in humans and primates and because many organisms, like *Drosophila*, have only a single PANK [8]. In mice, the PANK2 homolog protein was reported to localize in the cytosol [9]; a PANK2 knockout mouse exhibited reduced growth, retinal degeneration, and male infertility, but no movement disorders or signs of iron accumulation in the brain [10]. However, a pantothenic acid-deficient diet caused movement disorders in the mice without iron accumulation in the basal ganglia [11]. In accordance with these results, suppression of the single PANK in *Drosophila* caused neurodegeneration [12] that could be rescued by pantethine [13], but no neuronal iron accumulation was observed.

Given the lack of good animal models, cells derived from patients themselves can be used as an alternative approach for PKAN research and evaluation of potential therapies. Previous works with fibroblasts from PANK2 mutant patients indicated that an alteration of the cellular oxidative status and iron homeostasis can be detected in these cells [14].

In this manuscript, we propose that skin fibroblasts and induced neurons derived from PKAN patients represent unique cellular models for the study of the molecular mechanisms that may lead to iron accumulation and neurodegeneration in PKAN. Our findings suggest that PANK2 mutant fibroblasts and induced neurons recapitulate the abnormal iron metabolism seen in many cell types in patients with NBIA.

Material and Methods

Reagents

Monoclonal Anti-Actin antibody, Sudan Black, Prussian Blue, sodium pantothenate, Luperox® DI (tert-Butyl peroxide), deferiprone, and trypsin were purchased from Sigma Chemical Co. (St. Louis, MO). Mitosox™, MitoTracker Red CMXRos, DAPI and Hoechst 3342, were purchased from Invitrogen/Molecular Probes (Eugene, OR). Anti-cytochrome c antibodies and anti-MAP2 were purchased from PharMingen (BD Bioscience, San Jose, CA). Anti-transferrin receptor 1 (TfR1), anti-ferritin light-chain, anti-divalent metal transporter 1 (DMT1), NFS1, anti-PANK1, and anti-PANK2 were purchased from Santa Cruz Biotechnology (Santa Cruz, CA). Anti-iron-responsive element-binding protein 1 (IRP-1), anti-Tau clone HT7, and anti-PANK3 were purchased from Thermo-Fisher (Waltham, MA). OxyBlot Protein Oxidation Detection Kit was acquired from Merck (Darmstadt, Germany). MitoPeDPP was purchased from Dojindo Molecular Technologies, Inc. (Rockville, MD). A cocktail of protease inhibitors (complete cocktail) was purchased from Boehringer Mannheim (Indianapolis, IN). The Immun Star HRP substrate kit was from Bio-Rad Laboratories Inc. (Hercules, CA).

Ethical Statements

Approval of the ethical committee of the Hospital Universitario Virgen Macarena y Virgen de Rocío de Sevilla (Spain) was obtained, according to the principles of the Declaration of Helsinki and all the International Conferences on Harmonization and Good Clinical Practice Guidelines.

Cell Culture

We used primary skin fibroblasts from three unaffected subjects (controls 1, 2, and 3, two adults and one neonatal) purchased from ATCC and three patients from the Movement Disorder Unit of Hospital Universitario Virgen del Rocío, Sevilla, Spain, and from the Movement Disorders Bio-Bank available at the Neurogenetics Unit of the Neurological

Institute "Carlo Besta" (INCB), Milan, Italy. One patient (P1) is double heterozygous carrier of changes in position c.747dup (p.Arg249ProfsX43) that causes a stop codon and c.1475C>G (p.Ala492Gly) that causes a missense mutation, which is predicted to be damaging by prediction tools such as PolyPhen2 [15]. The second patient (P2) is double heterozygous carrier of changes in position 240–241delCA and T217I (650C>T), which have been previously described [16]. The third patient (P3) P3 carries a homozygous mutation c.1259delG causing a frameshift p.F419fsX472 [14]. Control values represent means ± SD for three control fibroblast cell lines. Fibroblasts were grown in DMEM (Sigma) supplemented with 10% FBS (Sigma), 100-mg/ml streptomycin, 100-U/ml penicillin, and 4-mM L-glutamine (Sigma). All the experiments were performed with fibroblasts cell cultures with a passage number < 10.

Cell Morphology

Cell morphology was evaluated by light microscopy. Images were analysed using the ImageJ software (National Institutes of Health, USA).

Iron and Lipofuscin Accumulation

Iron accumulation was examined by Perls' Prussian Blue staining [17]. Perls' staining was quantified in a microplate reader (Polar star Omega, BMG Labtech) and by light microscopy. Images and quantification analysis from light and fluorescence microscopy were performed by using the ImageJ software.

Lipofuscin accumulation was evaluated by Sudan Black B (SBB) staining as previously described [18]. SSB staining quantification was performed in a microplate reader and by light microscopy. Autofluorescence detection was performed by fluorescence microscopy (excitation 366 nm; emission 420–600 nm). Emission spectra of lipofuscin granules were obtained by confocal laser scanning microscopy (Nikon A1R, Shinagawa, Tokyo, Japan). Excitation laser source 405 nm. The spectra were detected in 5-nm steps. The emission spectra were recorded in 10 lipofuscin granules in 20 cells.

Lipofuscin Purification and Scanning Electron Microscopy with Energy Dispersive X-ray Spectroscopy (SEM/EDX)

Lipofuscin was isolated using a method described by Boulton and Marshall [19]. All experimental steps were carried out on ice with prechilled buffers, and all centrifugation steps were performed at 4 °C. Briefly, cell pellets were homogenized in a Dounce homogenizer and disrupted by sonication for 30 s set at 4 °C using a Branson Ultrasonics Sonifier S-450 in the presence of disruption buffer (50-mM Hepes, 0.25-M sucrose, 5-mM EDTA, 0.1-M potassium acetate, pH 7.5) supplemented with protease inhibitors (complete, Protease Inhibitor Cocktail Tablets/Roche Applied Science, Mannheim, Germany). Cellular debris was removed by centrifugation at 60 ×*g* for 7 min. The resulting supernatant was removed and then centrifuged (6000 ×*g*; 10 min). The pellet was resuspended in disruption buffer, and the suspension was layered on top of a discontinuous gradient consisting of five different concentrations of sucrose in disruption buffer: 1.6, 1.5, 1.4, 1.2, 1.0, and 0.25 M. Gradient separation was achieved by centrifugation at 100,000 ×*g* for 1 h in a swing-bucket rotor (TSL-55, Beckman Coulter, Fullerton, CA, USA). The lipofuscin-containing interface of the first sucrose gradient was identified by its characteristic fluorescence excitation/emission spectrum in a Cary Eclipse Fluorescence Spectrophotometer (Agilent, Santa Clara, CA, USA). Isolated lipofuscin was spread on a conductive carbon tape and dried before vacuum. Then, lipofuscin granules were analysed. SEM/EDX was performed at 20 kV with a Hitachi S-4800 SEM-FEG (Minato-ku, Tokyo, Japan) equipped with a Bruker X-FLASH 4010 detector (Billerica, MA, US) with a 133-eV resolution at the Mn K_α line. The analysis of EDX spectra were carried out by the Origin 2018 software (Originlab Corp. Northampton, MD, USA) by using the standardless Cliff-Lorimer's method, as described in previous reports [20]. The results are expressed as mole fractions in atomic percent (at%) and weight fractions (wt%).

Iron Determination by Ferrozine and Inductively Coupled Plasma Mass Spectrometry (ICP-MS) Assays

Iron levels in cell extracts were also determined by a Ferrozine assay [21] and ICP-MS [22]. Calibration was performed for six standards and the correlation coefficients (r) ranged from 0.98 to 0.99. Elemental concentrations are shown in nmol Fe^{2+}/μg protein. Values are shown as means ± SD (standard deviation) for three independent experiments.

Immunoblotting

Western blotting was performed using standard methods. After protein transfer, the membrane was incubated with various primary antibodies diluted 1:1000 and then with the corresponding secondary antibody coupled to horseradish peroxidase at a 1:10000 dilution. Specific protein complexes were identified using the Immun Star HRP substrate kit (Biorad Laboratories Inc., Hercules, CA, USA).

Immunofluorescence Microscopy

Fibroblasts were grown on 1 mm width (Goldseal No. 1) glass coverslips for 24–48 h in DMEM containing 20% FBS. Cells were rinsed once with PBS, fixed in 3.8% paraformaldehyde

for 5 min at room temperature and permeabilized in 0.1% saponin for 5 min. For immunostaining, glass coverslips were incubated with primary antibodies diluted 1:100 in PBS, 1–2 h at 37 °C in a humidified chamber. Unbound antibodies were removed by washing the coverslips with PBS (three times, 5 min). The secondary antibody, a FITC-labelled goat anti-mouse antibody, or a tetramethyl rhodamine goat anti-rabbit (Molecular Probes), diluted 1:100 in PBS, were added and incubated for 1 h 37 °C. Coverslips were then rinsed with PBS for 3 min, incubated for 1 min with PBS containing Hoechst 33342 (1 μg/ml), and washed with PBS (three 5-min washes). Finally, the coverslips were mounted onto microscope slides using Vectashield Mounting Medium (Vector Laboratories, Burlingame, CA, USA) and analyzed using an upright fluorescence microscope (Leica DMRE, Leica Microsystems GmbH, Wetzlar, Germany). Colocalization studies were performed using a DeltaVision system (Applied Precision; Issaquah, WA) with an Olympus IX-71 microscope (Olympus Corporation, Shinjuku, Tokyo, Japan).

Electron Microscopy

Fibroblasts were fixed for 15 min in the culture plates with 2% glutaraldehyde in culture medium, then for 30 min in 2% glutaraldehyde–0.1-M sodium cacodylate buffer, pH 7.4. They were then washed three times in sodium cacodylate 0.1 M for 10 min and then post-fixed with 1% OsO_4 in 0.1-M sodium cacodylate buffer for 30 min. After dehydration in increasing concentrations of ethanol, 5 min for each step: 30, 50, 70, and 95%, embedded in Durcupan® Fluka and polymerized at 60 °C for 48 h. Then, 1-μm sections were stained with toulidin blue, and 60–80-nm sections were cut with an ultramicrotome Leica UM6. The ultrathin sections were observed without uranyl acetate and lead citrate staining to avoid artifactual images and precipitates on a Zeiss Libra 120 transmission electron microscope.

Analysis of Cell Death

Viable cells were counted from their normal cell and nuclear morphology and exclusion of propidium iodide under a phase-contrast and fluorescence microscope at ×100 magnification. In each case, 10 random fields and more of 500 cells were counted. Cell death was determined by measuring LDH release in the medium using the CytoTox-ONE™ Homogeneous Membrane Integrity Assay kit (Promega, Madison, WI) according to the manufacturer's instructions.

Iron Metabolism

To examine the effect of selected compounds from the initial screening test on NBIA mutant fibroblasts, iron homeostasis will be studied. Labile iron pool (LIP) determination was carried out as previously described [14]. Briefly, fibroblasts were plated in 96-well plates. Cells were incubated in medium supplemented with 1-mg/ml BSA and 0.25-μm calcein-AM at 37 °C for 15 min. After two washes with Hank's balanced salt solution (HBSS), cells were maintained in HBSS supplemented with 10-mm glucose for 10 min. Basal fluorescence was measured using a POLARstar Omega Microplate Reader at 485 (excitation) and 535 nm (emission). Cells were then supplemented with the specific iron chelator salicyladehyde isonicotinoyl hydrazone (0.1 mM) for 15 min. Fluorescence was followed during incubation with the chelator and when a plateau was reached, the value was considered to be the LIP value. Finally, the results were normalized to the protein content.

IRP-1, transferrin receptor 1 (TfR1), ferritin, and DMT1 expression levels were determined by Western blotting.

Mitochondria Isolation

Subcellular fractionation was performed following the protocol by Abcam (http://www.abcam.com/ps/pdf/protocols/subcellular_fractionation.pdf) according the protocol provided by Dr. Richard Patten. In brief, cells were lysed with a subcellular fractionation buffer (250-mM sucrose, 20-mM HEPES, 10-mM KCl, 1.5-mM $MgCl_2$, 1-mM EDTA, 1-mM EGTA, 1-mM DTT, protease inhibitor coctail (III)), and cell lysates were centrifuged (720 ×*g*). The pellet was washed in fractionation buffer and resuspended in nuclear buffer (standard lysis buffer containing 0.1% SDS); this is the nuclear fraction. The supernatant was re-centrifuged at a higher speed (100,000 ×*g*); the supernatant, after ultra-centrifugation, is the cytoplasmic fraction. The pellet was washed with fractionation buffer; this is the membrane fraction.

Determination of CoA Levels in Mitochondria CoA levels in the mitochondrial fraction were analysed by HPLC as previously described [23]. The concentrations of standard CoA were determined using a molar absorbance of 16,000 at 260 nm. These agents were dissolved in 50-mmol/L KH_2PO_4–K_2HPO_4 buffer (pH 7.0). Frozen mitochondrial fractions resuspended in KH_2PO_4–K_2HPO_4 were sonicated (10% amplitude during 10 s). The homogenates were centrifuged at 12,000 ×*g* for 10 min at 4 °C. The supernatant was passed through a 0.45-μm filter (Millipore, Bedford, MA), and the filtrate (10 μl) was injected directly into the HPLC system. The content of CoA was measured as follows. The method employed a Shim-pack VP-ODS (150 mm L × 4.6 mm I.D., 5 μm) eluted with 100-mmol/L NaH_2PO_4 and 75-mmol/L CH_3COONa (pH was adjusted to 4.6 by the addition of concentrated H_3PO_4)–acetonitrile (94:6, *v*/*v*) at a flow rate of 1.0 ml/min. The ultraviolet (UV) detector was set at 259 nm. The standards of CoA eluted at approximately 3.5 min under these conditions. Mitochondrial proteins were

determined using the Lowry assay [24]. CoA values were referred to protein content in the mitochondrial fraction.

Bioenergetic and Oxidative Stress Analysis

Mitochondrial respiratory function of control and PKAN fibroblasts were measured using mito-stress test assay by XF24 extracellular flux analyzer (Seahorse Bioscience, Billerica, MA).

Cells were seeded at a density of 3×10^4 cells/well in XF24 cell culture plates in 100-μL growth medium (DMEM medium containing 20% FBS) and placed in 37 °C incubator with 5% CO_2. After 24 h incubation, growth medium from each well was removed, leaving 50 μL of media. Then, cells were washed twice with 1000 μL of pre-warmed assay medium (XF base medium supplemented with 10-mM glucose, 1-mM glutamine, and 1-mM sodium pyruvate; pH 7.4) and 450 μL of assay medium (500 μL final) was added. Cells were incubated in 37 °C incubator without CO_2 for 1 h to allow pre-equilibrating with the assay medium. Mitochondrial functionality was evaluated by sequential injection of four compounds that affect bioenergetics. The final concentrations of injections were 1-μM oligomycin, 2-μM FCCP (carbonyl cyanide-4-trifluoromethoxy-phenylhydrazone), 1-, and 2.5-μM rotenone/antimycin A. The best concentration of each inhibitor and uncoupler, as well as the optimal cells seeding density, were determined in preliminary analyses. A minimum of five wells per treatment were utilized in any given experiment. This assay allowed for an estimation of basal respiration, maximal respiration, and spare respiratory capacity.

Oxidized proteins will be detected using the Oxyblot Protein Oxidation Detection Kit following the manufacturer's instructions. Lipid peroxidation will be assessed by measuring the oxidation of MitoPeDPP according to the manufacturer's instructions. MitoPeDPP a cell-membrane-permeable probe, perylene-based dye. It specifically localizes in mitochondria due to the triphenylphosphonium moiety introduced. Mitochondrial localization of MitoPeDPP signal was confirmed by fluorescence microscopy of samples incubated with MitpPeDPP and MitoTracker Red CMXRos (100 nM, 30 min), a mitochondrial potential-dependent dye. Colocalization of both markers was assessed by the DeltaVision software calculating the Pearson coefficient of correlation.

Determination of Heme Content

Heme content was measured in fibroblasts from patients and controls as previously described [25]. Briefly, the cells were washed with phosphate-buffered saline and dissolved in 0.25 ml of 98% formic acid and incubated for 15 min. The heme content was evaluated by analysing the clear supernatant at 400 nm, with an extinction coefficient of $1.56 \times 10^5 \times M^{-1} \times cm^{-1}$. The data were normalised to protein content as determined by the BioRad Protein Assay (BioRad).

Analysis of Mitochondrial Network

The amount of mitochondrial fragmentation was evaluated using the IFDOTMETER software [26]. For each experimental condition, a total of 100 images collected in three different experiments were used to calculate the number of small rounded mitochondria per cell. Length or ratio between the major and minor axis of the mitochondrion and degree of circularity were taken into account.

Generation of Induced Neurons from Fibroblasts by Direct Reprogramming

Neurons were generated from patient and control fibroblasts by direct reprogramming as previously described by Drouin-Ouellet et al. [27, 28]. Controls and patients-derived fibroblasts were plated onto 0.1% gelatin-coated 24-well plates or μ-Slide 4 Well Ibidi plates (2.8e4 cells/cm^2). The day after, dermal fibroblasts were transduced with one-single lentiviral vector containing neural lineage-specific transcription factors (Acsl1 and Brn2) and two shRNA against the RE1-silencing transcription factor (REST) complex, generated as previously described [29]. The plasmid was a gift from Dr. Malin Parmar (Developmental and Regenerative Neurobiology, Lund University, Sweden). Transduction was performed at a multiplicity of infection (MOI) of 30. The day after, the cells were switched into fresh fibroblast medium and after a further 48 h, the medium was replaced with neural differentiation medium (NDiff227; Takara-Clontech) supplemented with neural growth factors and small molecules at the concentrations previously described [27]: LM-22A4 (2 μM, R&D Systems), GDNF (2 ng/ml, R&D Systems), NT3 (10 ng/ml, R&D Systems), db-cAMP (0.5 mM, Sigma), CHIR99021 (2 μM, Sigma), SB-431542 (10 μM, R&D Systems), noggin (50 ng/ml, R&D Systems), LDN-193189 (0.5 M, Sigma), and valproic acid sodium salt (VPA; 1 mM, Sigma). Half of the neuronal differentiation medium was replaced every 2–3 days. Eighteen days post-infection, the medium was replaced with neuronal medium supplemented with only the growth factors until the end of the conversion. The medium was changed every 2–3 days for a further 10 days. Neuronal cells will be identified by the expression of Tau or MAP2. DAPI+ and Tau+/MAP2+ cells were considered induced neurons. Conversion efficiency was calculated as the number of Tau+ cells over the total number of fibroblasts seeded for conversion. Neuronal purity was calculated as the number of Tau+ cells over the total cells in the plate after reprogramming.

Statistical Analyses

The data are reported as the mean ± SD values or as representative of at least three independent experiments. Statistically significant differences between controls and patients were determined in all the experiments by one-way ANOVA analyses and by Student's t test; a p value < 0.05 was considered statistically significant.

Results

Expression Levels of PANK2 Are Reduced in Fibroblasts Derived from PKAN Patients

We analyzed PANK2 expression levels in fibroblast cell lines derived from three PKAN patients and three healthy subjects. Two PKAN patients, P1 and P2, carried double heterozygous mutations (one allele harbors a stop codon mutation and the other a missense mutation) while patient P3 carried a homozygous mutation carrying a frame shift mutation that results in a truncated PANK2 protein [14]. As shown by Western blot analysis in Fig. 1a, b, PANK2 expression levels (band around 48 kDa) were markedly reduced in patients P1 and P2 and practically absent in P3, while normal levels were present in control fibroblasts. To compensate the deficiency of PANK2, expression levels of PANK1 were remarkably increased in all three patient fibroblasts. However, expression levels of PANK3 were not significantly different.

Fibroblasts from PKAN Patients Showed Altered Cell Morphology and Accumulation of Iron and Lipofuscin

We then examined cell morphology and iron and lipofuscin accumulation in PKAN fibroblasts. Examination of cell morphology by bright-field microscopy revealed that PKAN fibroblasts showed characteristic morphological changes that accompany replicative senescence in cultured cells (Fig. 1c). The increased cell size was quantified by determining cell perimeter. This parameter was significantly increased in PKAN fibroblasts compared to control cells (Fig. 1d).

As altered iron metabolism is one of the main characteristic of PKAN mutations, we next examined intracellular iron accumulation by Prussian Blue staining in three control and PKAN fibroblasts (Fig. 1e). Iron staining was significantly increased in PKAN affected cells (Fig. 1e, f and Supplementary Fig. S1a). Fibroblasts harbouring the MERRF (myoclonic epilepsy with ragged-red fibers) mutation A8344G, a mitochondrial disease with neurological involvement but without iron accumulation, as well as P1 fibroblasts treated with deferiprone, an iron chelating drug, were used as a negative control. To confirm the abnormal cellular iron content in PKAN fibroblasts, we next determined intracellular iron levels by a colorometric ferrozine-based assay [21]. All three patient affected cells showed increased total iron levels (Supplementary Fig. S1b). The basal amounts of iron in control cultures were approximately 50-nmol iron per mg protein, while iron content was in the range of 80–120 iron per mg protein in PKAN fibroblasts.

As abnormal accumulation of lipofuscin in NBIA patients has been reported in several cell types derived from NBIA patients [30, 31] and lipofuscin accumulation can result from lipid peroxidation, a process stimulated by iron [32, 33], we next examined the presence of lipofuscin by autofluorescence analysis, Sudan Black staining, and electron microscopy analysis in control and PKAN fibroblasts. PKAN mutant cells showed increased autofluorescence and increased Sudan Black staining compared with control cells suggesting lipofuscin accumulation (Fig. 2a, b). Increased intracellular lipofuscin granules in PKAN fibroblasts were confirmed by electron microscopy examination (Fig. 2c). The quantification of autofluorescence, Sudan Black staining, and lipofuscin granules is showed in Supplementary Fig. S2. Autofluorescence in patient fibroblasts was significantly reduced after treatment with deferiprone, suggesting that iron is contributing to the accumulation of the autofluorescent lipofuscin-like material (Supplementary Fig. S3). Furthermore, to confirm the lipofuscin-like characteristic of the aggregates, the fluorescence spectral characteristics of lipofuscin granules were performed by confocal laser scanning microscopy. Under excitation at 405 nm, lipofuscin granules showed an emission peak at 510–520 nm (Supplementary Fig. S4). These observed spectra are consistent with the reported characteristics of lipofuscin granules obtained by Bindewald-Wittich et al. in retinal pigment epithelial cells by confocal microscopy [34].

SEM/EDX, a widely applied elemental microanalysis method capable of identifying all elements in the periodic table except H, He, and Li [35], was used to determine the chemical composition of lipofuscin isolated from P1 fibroblasts. High-precision EDX microanalysis revealed that lipofuscin granules contain a high iron weight fraction (about 5%) (Fig. 2d and Supplementary Table 1). A quantitative analysis of EDX spectra of four lipofuscin granules is also shown in Supplementary Table 2.

Pantothenate Treatment Restored Cell Morphology and Reduced Iron/Lipofuscin Accumulation in Fibroblasts Derived from PKAN Patients Depending on the Type of PANK2 Mutation

To examine if any residual PANK2 enzyme could be stabilized and correct the pathological alterations in PKAN fibroblasts, control and affected cells were treated with increasing concentration of pantothenate (50–500 μM) and cell morphology and iron/lipofuscin accumulation

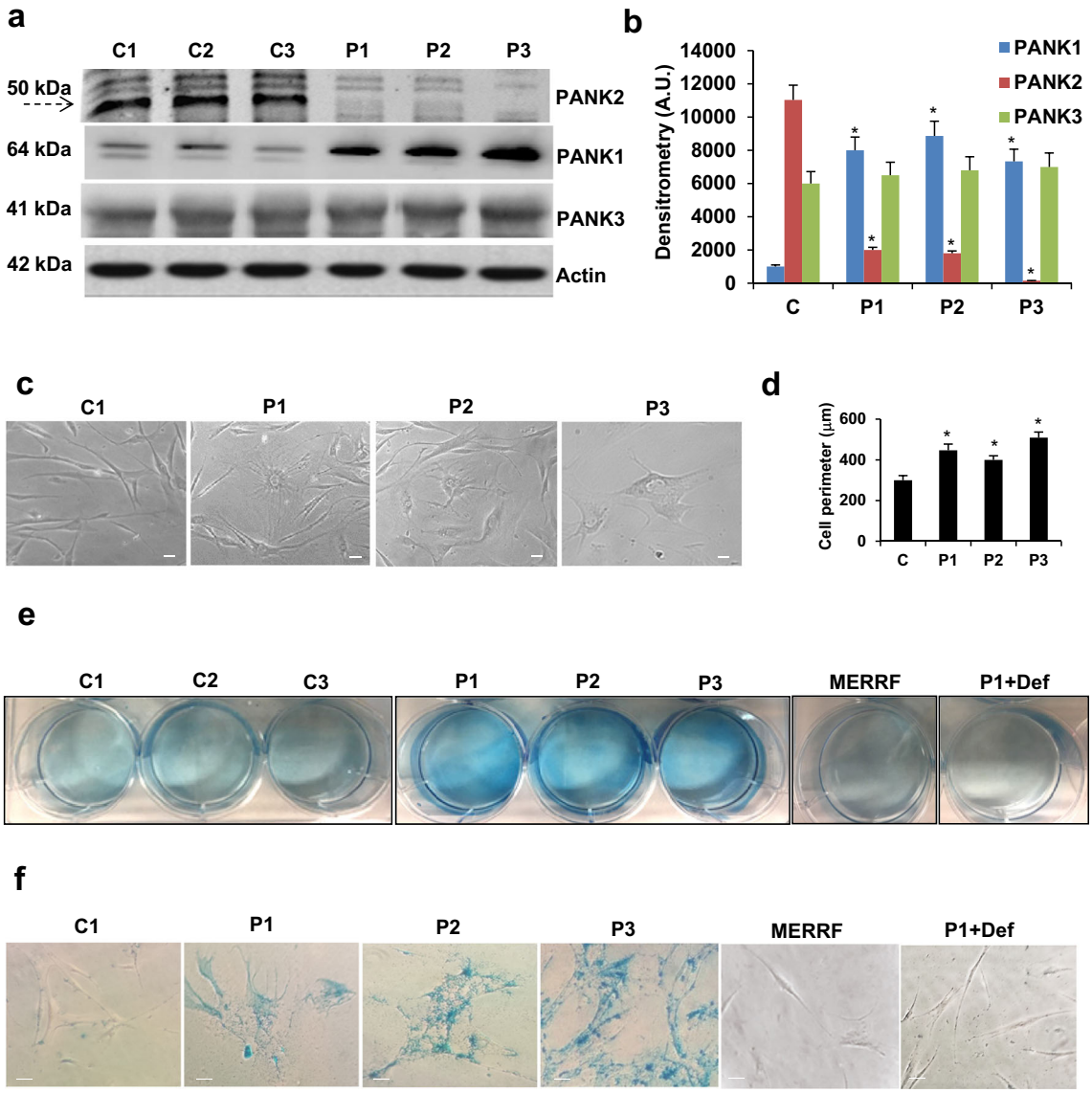

Fig. 1 Expression levels of PANK1, PANK2 AND PANK3 in PKAN fibroblasts. **a** Immunoblotting analysis of cellular extracts from control (C) and patients P1, P2, and P3 fibroblasts. Protein extracts (50 μg) were separated on a SDS polyacrylamide gel and immunostained with antibodies against PANK1, PANK2, and PANK3. Dashed arrow points to PANK2 mature peptide of 48.5 kDa. Actin was used as a loading control. **b** Densitometry of the Western blotting. For control cells (C), data are the mean ± SD of the three control cell lines. **c** Bright-field images of control (C1) and PKAN fibroblasts. Scale bar = 15 μm. **d** Cell perimeter of control and PKAN fibroblast. **e** Prussian Blue staining of 3 control cell lines (C1, C2, and C3) and PKAN fibroblasts (P1, P2, P3) cultured in 6-well plates as described in the "Material and Methods." The staining solution was removed to visualize the stained cells on the bottom of the wells. **f** Bright-field pictures at high magnification of control (C1) and patients P1, P2, and P3 after Prussian Blue staining. Fibroblasts harbouring the MERRF (myoclonic epilepsy with ragged-red fibers) mutation A8344G, a mitochondrial disease, as well as P1 fibroblasts treated with 100-μM deferiprone (Def) for 96 h were used as a negative control. Scale bar = 15 μm. Data represent the mean ± SD of three separate experiments. $^{*}p < 0.01$ between PKAN patients and controls. A.U., arbitrary units

were evaluated. As it is it illustrated in Fig. 3a, b, pantothenate treatment reduced drastically iron accumulation in patients 1 and 2 (P1 and P2) but not in patient 3 (P3) in which the expression of PANK2 is totally absent and the mutation produces a truncated protein. In pantothenate-responder fibroblasts, the effect of pantothenate was dose and time dependent (Fig. 3c). To corroborate these results, intracellular iron content was determined by ferrozine (Fig. 4a) and ICP-MS assays (Fig. 4b).

Altered cell morphology in PKAN fibroblast was also corrected by pantothenate treatment (500 μM) in responder affected cells, P1 and P2, but not in patient P3 (Fig. 5a, b).

Likewise, pantothenate treatment (500 μM) corrected the increased autofluorescence (Fig. 5c) and Sudan

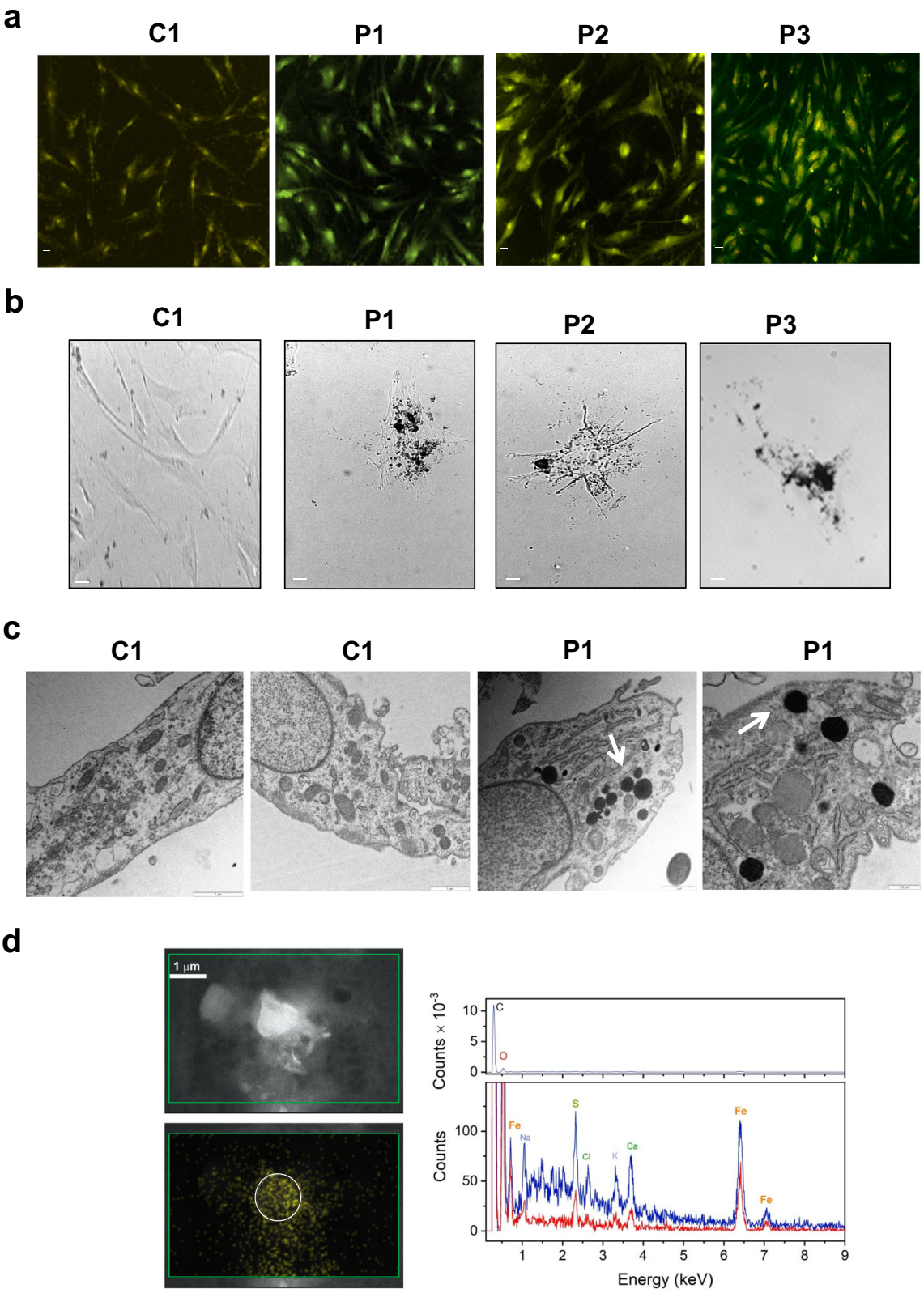

Black staining (Supplementary Fig. S5) in PKAN responder fibroblasts, P1 and P2, but not in P3. Lipofuscin elimination in responder affected cells after pantothenate treatment was also confirmed by light and electron microscopy examination in patient P1 (Fig. 6 and Supplementary Fig. S6).

◀ **Fig. 2** Lipofuscin accumulation in PKAN fibroblasts. **a** Representative autofluorescence images of control (C1) and PKAN fibroblasts. Scale bar = 30 μm. **b** Sudan Black staining of control cells lines (C1) and PKAN fibroblasts (P1, P2, P3) as described in "Material and Methods." Scale bar = 15 μm. **c** Electron microscopy images of control (C1) and P1 fibroblasts. White arrows, lipofuscin granules. Scale bar = 1 μm and 0.5 μm. **d** Scanning electron microscopy with energy dispersive X-ray spectroscopy (SEM/EDX) of an isolated lipofuscin granule. Primary electron beam energy was set to 20 kV. Upper left, image of a selected region (green square), lower left, overlay of the elemental map associated to the Fe Kα transition energy. White circle represents a spot selected for analysis. Right, EDX spectra of the overall region (blue spectrum, green squared window in upper let panel) and the selected spot (red spectrum). The presence of X-ray emission at the Fe Lβ1/α12, Kα and Kβ transition energies are labelled in orange

Pantothenate Treatment Prevented Protein Carbonylation and Mitochondrial Lipid Peroxidation in Responder PKAN Fibroblasts

We then determined cellular oxidative status and its relationship with pantothenate treatment response by treating control and PKAN fibroblasts with pantothenate (500 μM). The content of carbonylated proteins in the pantothenate-treated and untreated cellular extracts was then evaluated by Oxyblot (Fig. 7a, b). The results confirmed that untreated PKAN fibroblasts showed increased carbonylated protein levels compared to control cells and that pantothenate treatment was able to reduced carbonylated proteins in responder mutant fibroblasts P1 and P2, but not in P3 fibroblasts.

The levels of mitochondrial lipid peroxidation in pantothenate-treated and untreated fibroblasts were assessed by MitoPeDPP, which is specifically-oxidized by lipophilic peroxides in mitochondria [36]. PKAN fibroblasts showed increased mitochondrial lipid peroxidation levels compared to control cells, and pantothenate treatment (500 μM) was able to reduce them in responder mutant fibroblasts P1 (Fig. 7c, d). Colocalization assays showed that indeed the MitoPeDPP signal colocalizes with mitochondrial markers (Supplementary Fig. S7a and S7b).

Pantothenate Restored Cell Bioenergetics and Mitochondrial Network Alterations in Responder PKAN Fibroblasts

Given that PANK2 is a mitochondrial enzyme, we further investigated the ability of pantothenate treatment to restore cellular energy requirement in PKAN responder mutant cells. For that purpose, the oxygen consumption rate (OCR) was examined in patient 1 (Supplementary Fig. S8). Fibroblasts from patient P1 showed reduced basal, maximal, and spare respiration compared to the control cells. This reduced respiratory ability is in agreement with the presence of mitochondrial dysfunction. Pantothenate treatment (500 μM) significantly increased all the altered bioenergetics parameters in P1 fibroblasts.

We next investigated mitochondrial morphology after labeling mitochondria with anti-cytochrome c antibody and examination by fluorescence microscopy. Representative images of these classes of mitochondrial morphology are shown in (Supplementary Figs. S9 and S10). A total of 100 different images were obtained and quantified for each sample. The amount of mitochondrial fragmentation was evaluated using the IFDOTMETER software. The mitochondrial network of PKAN patients with loss-of-function mutations was more fragmented than controls, indicating an impaired bioenergetic profile.

Pantothenate Treatment Protected from Induced-Cell Death in Responder PKAN Fibroblasts

The beneficial effect of pantothenate on responder PKAN fibroblasts was also confirmed by examining the protective effect of pantothenate treatment on cell death assays induced by rotenone or iron supplementation. Pantothenate treatment (500 μM) significantly protected mutant cells from the toxic effects of both rotenone and iron supplementation (Supplementary Fig. S11).

Pantothenate Treatment Stabilized Mutant PANK2 Expression Levels in Responder PKAN Fibroblasts

Given that pantothenate is the substrate of the PANK2 enzyme, we next examined if the treatment with pantothenate was able to stabilize the mutant enzyme in selected patients. Pantothenate treatment (500 μM) stabilized PANK2 expression levels in responder PKAN fibroblasts, P1 and P2, but not in non-responder P3 fibroblasts (Fig. 8a).

In agreement with these findings, pantothenate treatment (500 μM) increased CoA levels in mitochondria of responder P2 fibroblasts, which may contain residual PANK2 protein, but not in P3 fibroblasts which present a truncated version of the enzyme (Fig. 8b).

Pantothenate Treatment Corrects Iron Metabolism in Responder PKAN Fibroblasts

Perturbation of iron metabolism and distribution has been observed in PKAN [5]. To evaluate the effect of pantothenate treatment in mutant PKAN fibroblast, we assessed iron metabolism by examining the expression levels of key proteins involved in iron trafficking, storage, and regulation, such as DMT1, ferritin, TfR1, and IRP-1. In addition, the levels of LIP were also quantified by a calcein assay.

PANK2 mutant fibroblasts showed increased expression levels of DMT1 respect to control cells (Supplementary Fig. S12a). However, ferritin, TfR1, and IRP-1 expression

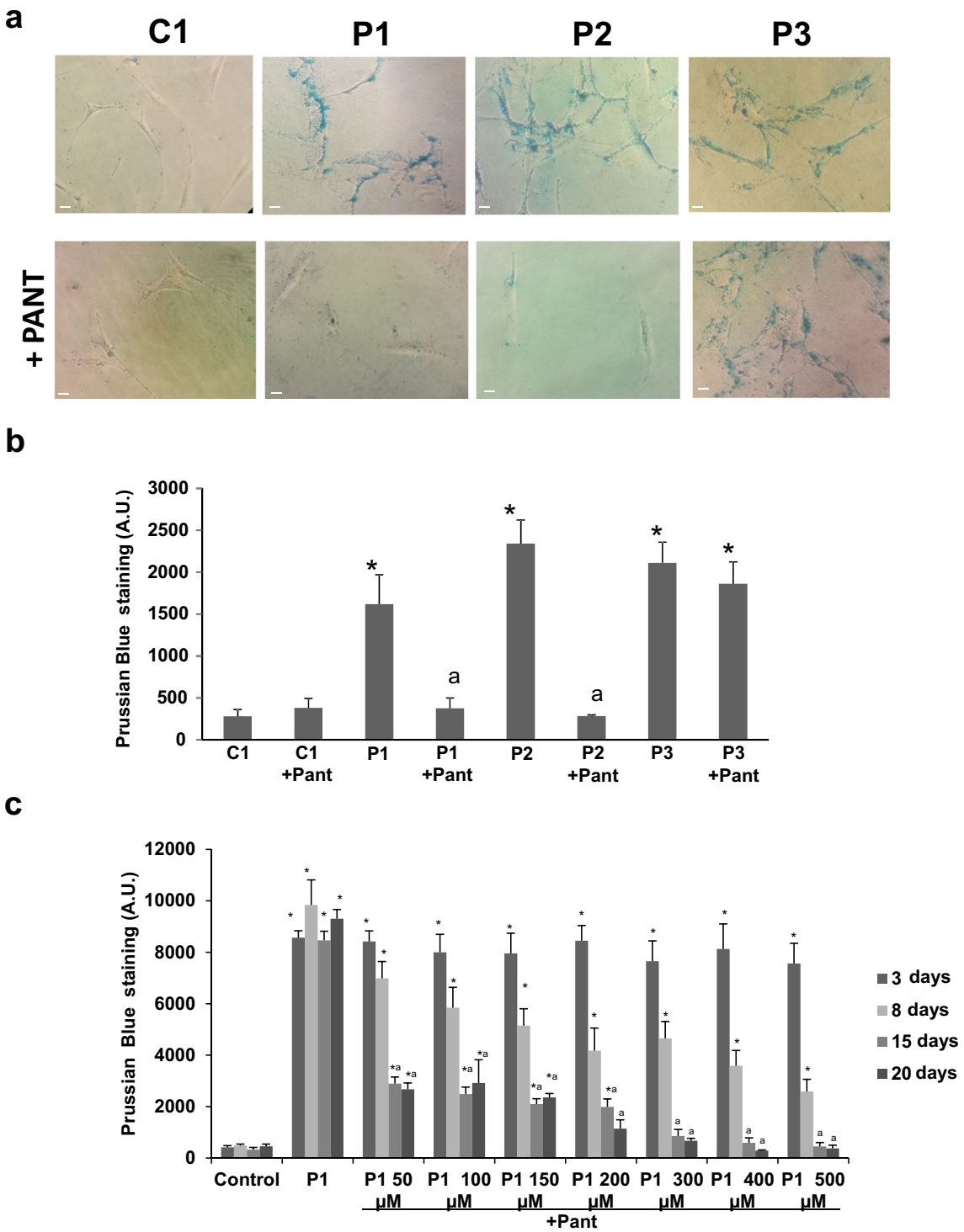

Fig. 3 Effect of pantothenate treatment on iron accumulation. **a** Control (C1) and PKAN fibroblasts (P1, P2, and P3) were treated with 500-μM pantothenate for 20 days. Then, cells were stained with Prussian Blue as described in the "Material and Methods" and examined by bright-field microscopy. Scale bar = 15 μm. **b** Quantification of Prussian Blue staining images were analyzed by the ImageJ software. **c** Quantification of Prussian Blue staining in control and a responder PKAN patient (P1) after the incubation with increasing concentrations of pantothenate (50–500 μM) during 3–20 days. Images were analyzed by the ImageJ software. $^{*}p < 0.01$ between control and PKAN fibroblats. $^{a}p < 0.01$ between untreated and treated fibroblasts. A.U., arbitrary units

levels were near to control values. Interestingly, LIP was dramatically reduced in mutant cells indicating paradoxically the low availability of free iron by PANK2 cells, although total iron was increased (Supplementary Fig. S12b). Both LIP and

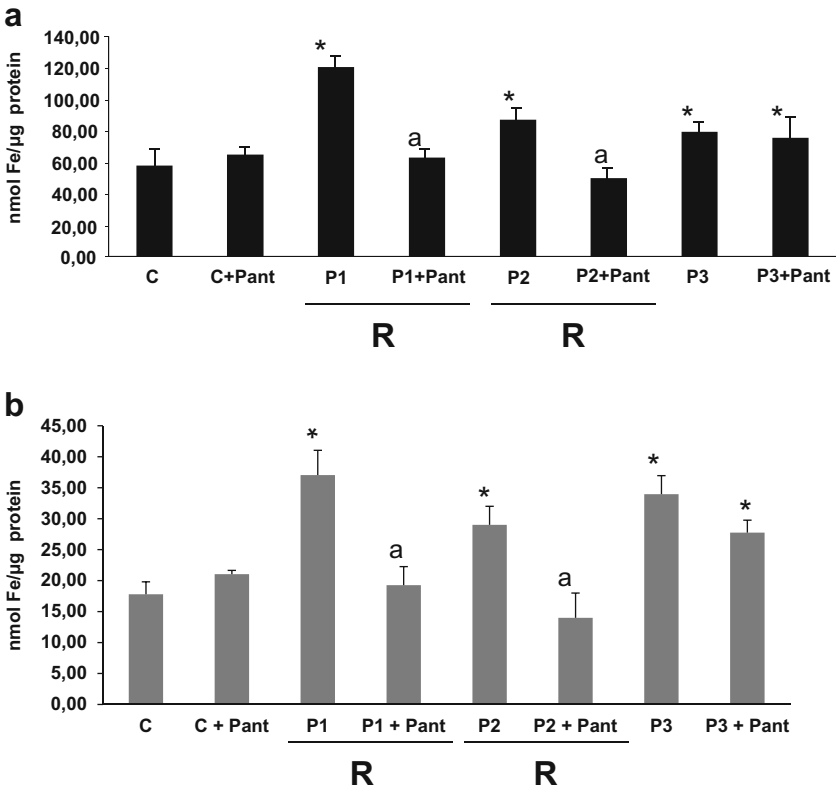

Fig. 4 Total iron content in PKAN fibroblasts. **a** Iron content determined by a ferrozine assay. Control and patient fibroblasts were incubated with pantothenate (500 µM) for 20 days. Total iron content of control (C) and PKAN patient fibroblasts (P1, P2, and P3) was determined by a ferrozine assay as described in "Material and Methods." **b** Iron content determined by ICP-MS. Total iron content of control and PKAN patients was determined by ICP-MS as described in "Material and Methods." For control cells, the data are the mean ± SD for experiments conducted on three different control cell lines. Data represent the mean ± SD of three separate experiments. $^{*}p < 0.05$ between control and PKAN fibroblats. $^{a}p < 0.01$ between untreated and treated cells. R = pantothenate responder fibroblasts

DMT1 expression levels were partially corrected after pantothenate treatment in responder fibroblasts.

As impaired iron metabolism in PKAN fibroblasts has been previously associated with impaired ISC (iron-sulphur cluster) and heme biosynthesis [14, 37], we next explore both the expression levels of NSF1, a protein required for of ISC assembly, and heme levels in control and PKAN fibroblasts. Expression levels of NSF1 were dramatically reduced in PKAN fibroblasts suggesting disorganization of the ISC complex (Supplementary Fig. S12a). Similarly, heme levels were significantly reduced in mutant PANK2 cells. Both NSF1 and heme levels were partially restored after pantothenate treatment in responder fibroblasts (Supplementary Fig. S12a and S12c).

Generation of Induced Neurons from Control and PANK2 Mutant Fibroblasts

To further demonstrate the beneficial effect of pantothenate in responder cells, control and patient fibroblasts were transdifferentiated to induced neurons by direct reprograming. For this, we employed a recently described method to express proneural genes Ascl1 and Blc2 and knock down REST complex by infecting control and PANK2 mutant fibroblasts with lentiviral vectors [27] (see "Materials and Methods"). Twenty-seven days after infection, cells exhibited a typical neuron-like morphology and showed positive immunoreactivity against Tau, a microtubule-associated protein found predominantly in neuronal axons of vertebrate brain, and microtubule associated protein 2 (MAP2), a neuron-specific protein that stabilizes microtubules (Supplementary Fig. S13a). In contrast, those undifferentiated cells did not show Tau or MAP2 staining and only showed the nuclear staining. We used Tau+/MAP2+ cells to evaluate neuronal conversion efficiency, which was almost 40% in control cells and 20% in PANK2 mutant cells (Supplementary Fig. S13b). Neuronal purity was approximately almost 35% in control cells and 55% in PANK2 mutant cells (Supplementary Fig. S13c).

To evaluate the beneficial effect of pantothenate treatment in mutant PKAN induced neurons we assessed iron accumulation by examining Prussian Blue staining in neuronal cells derived from patient P1 whose fibroblasts respond positively to pantothenate. PANK2 mutant induced neurons showed increased Prussian Blue staining indicating iron accumulation (Fig. 9a, b, c). As expected, iron accumulation was eliminated after pantothenate treatment (Fig. 9a, b, c).

Discussion

In this work, we studied the pathophysiology of PANK2 mutations in primary cultured fibroblasts derived from PKAN patients with clinical manifestations of neurological involvement. We assessed PANK2 expression deficiency, iron and lipofuscin

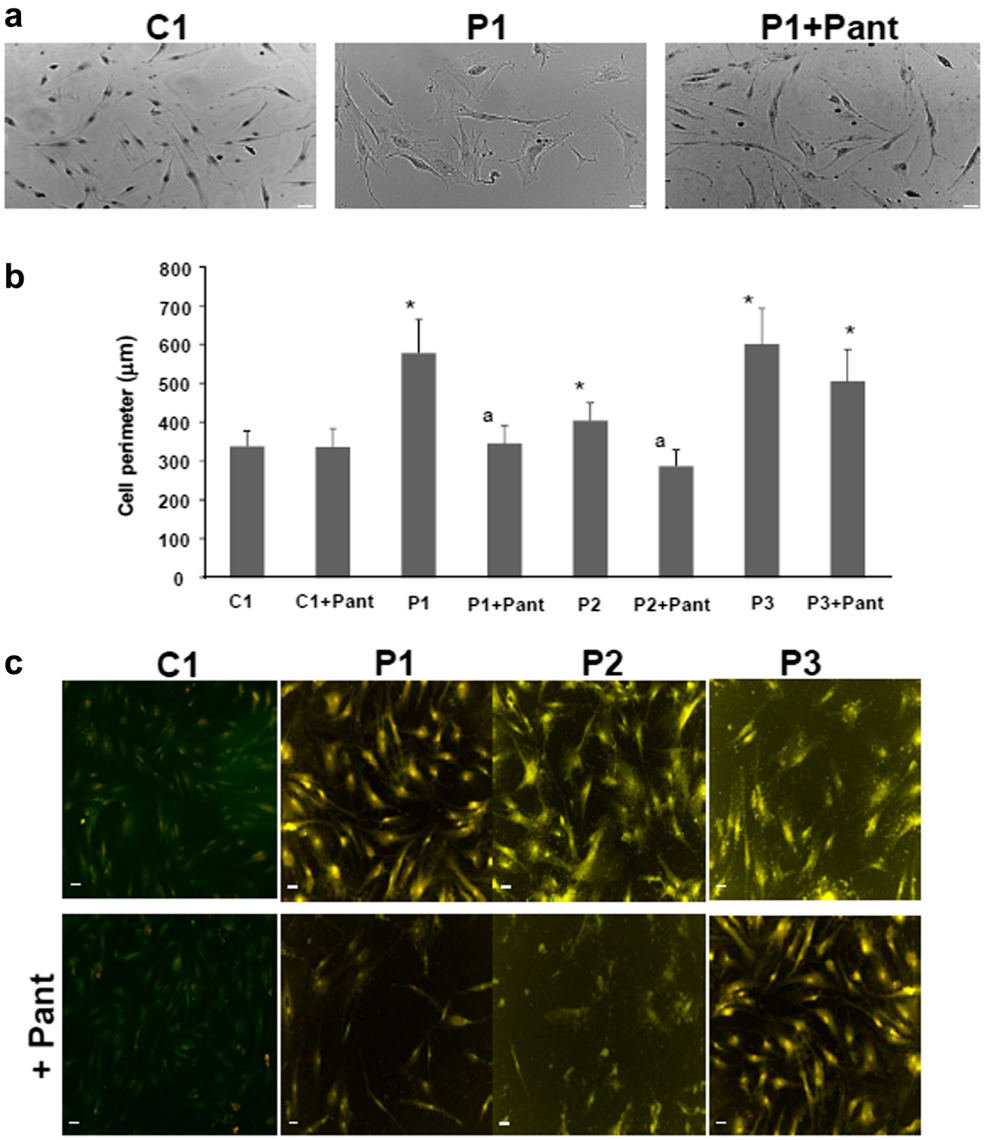

Fig. 5 Effect of pantothenate treatment on cell morphology and autofluorescence. **a** Cell morphology of control and PKAN fibroblasts. Representative light microscopy images of control (C1) and PKAN fibroblasts (P1) after 500-μM pantothenate (Pant) treatment for 20 days. Scale bar = 15 μm. **b** Cell perimeter of control and PKAN fibroblasts. Cell perimeter of control (C1) and PKAN fibroblasts (P1, P2, and P3) was determined by using ImageJ software. **c** Autofluorescence of control and PKAN fibroblasts. Autofluorescence images of control (C1) and PKAN fibroblasts (P1, P2, and P3) untreated and treated with 500-μM pantothenate (Pant) for 20 days. Scale bar = 15 μm. $^{*}p < 0.01$ between control and PKAN fibroblasts. $^{a}p < 0.01$ between untreated and treated cells

accumulation, and alterations in cell morphology as well as mitochondrial dysfunction and oxidative stress. Iron overload was confirmed by Prussian Blue staining, biochemical assays, and mass spectrometry. In turn, lipofuscin accumulation was determined by autofluorescence analysis, Sudan Black staining, and electron microscopy examination. Furthermore, iron accumulation was detected in induced neurons derived from mutant fibroblasts by direct reprogramming. We propose that these pathological alterations in PKAN fibroblasts and induced neurons can be useful for both understanding the underlying pathological mechanisms of the disease and the development of screening protocols for testing potential effective drugs in PKAN patients.

Interestingly, pantothenate treatment restored all pathological alterations including CoA levels in two responder mutant fibroblast cell lines (P1 and P2), but was not effective in a third one (P3). This differential response could be due to the different type of mutation in each fibroblast cell lines. P1 and P2 fibroblasts have residual PANK2 expression that was stabilized by pantothenate treatment, while PANK2 expression was absent in P3 fibroblasts (due to a frame shift mutation that produces a truncated protein) and it was not stabilized by pantothenate supplementation. The prevention of iron accumulation by pantothenate treatment was also demonstrated in induced neurons derived from responder fibroblasts.

The utilization of skin fibroblasts to reproduce some pathological effects of the disease has been amply reported [14, 38]. Recently, Ingrassia et al. have documented that fibroblasts derived from patients with beta-propeller protein-associated neurodegeneration, a different NBIA subclass,

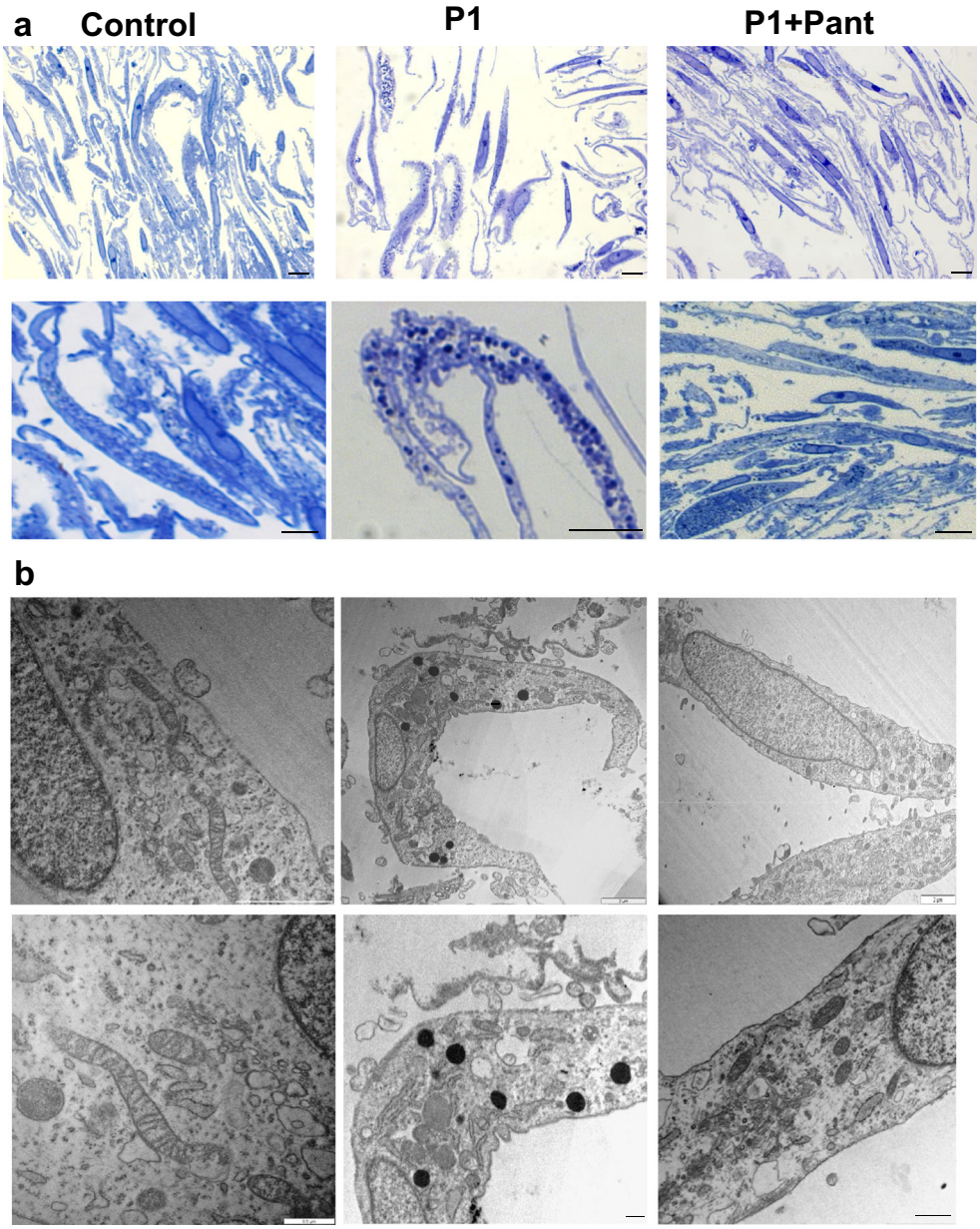

Fig. 6 Semithin sections and electron microscopy analysis in PKAN fibroblasts. Control (C1) and PKAN fibroblasts (P1) were treated with 500-μM pantothenate for 20 days. **a** Representative images of semithin sections of 1 μm stained with toluidine blue and visualized by light microscope. Scale bar = 15 μM. **b** Representative electron microscopy images of control (C1) and PKAN fibroblasts (P1) Top panel scale bar = 0.2 μm; bottom panel = 0.5 μm

accumulate iron that can be detected by specific staining protocols [39].

Our results clearly showed that iron is accumulated in fibroblasts and induced neurons derived from PKAN patients indicating that both cellular models can be very useful for the study of PKAN pathophysiology.

Previous works have demonstrated that PKAN-induced neurons by direct reprograming show alterations in mitochondrial membrane potential, signs of mitochondrial dysfunction, and altered oxidative status [38]. In our study, for the first time, we show that iron accumulation was also detected in PKAN induced neurons, which can be eliminated by pantothenate treatment in selected mutations.

Iron is an essential element for cell physiology, participating in a wide variety of cellular processes [40]. However, iron is a potential producer of ROS, and iron overload may promote cell damage by hydroxyl radical formation, which leads to protein/lipid oxidation and nucleic acid damage [41, 42]. Typically, Perls' staining of PKAN brain tissue shows a widespread perivascular deposition of iron largely confined to the globus pallidus [43]. Iron deposition also occurs to a lesser extent in the substantia nigra and other areas of the brain. Several hypotheses have been proposed to explain iron overload. One explanation is that intracellular iron accumulation results from neuronal apoptosis. Thus, it has been shown that ceramide-mediated apoptosis is dependent on increased

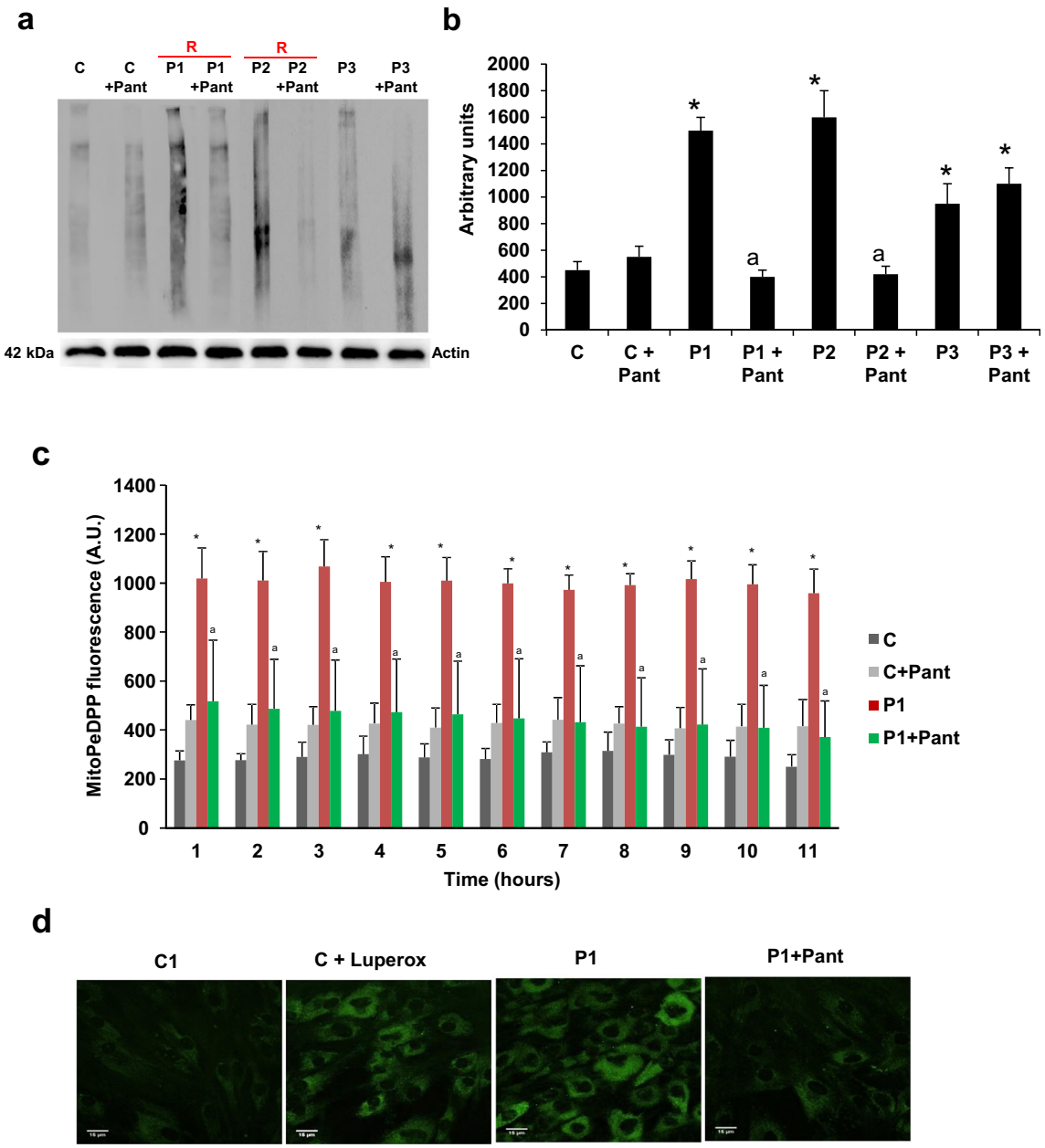

Fig. 7 Oxidative stress in PKAN fibroblasts. **a** Levels of carbonylated protein in control (C1) and PKAN fibroblast (P1, P2, P3) cellular extracts assayed by the OxyBlot Protein Oxidation Detection Kit. One representative of three independent experiments is shown. **b** OxyBlot quantification was performed by using the ImageJ software. **c** Mitochondrial lipid peroxidation assessed by MitoPeDPP in control (C1) and PKAN patient 1 fibroblasts (P1) untreated and treated with 500-μM pantothenate for 20 days. **d** Representative fluorescence images of control (C1) and P1 fibroblasts (MitoPeDPP) untreated and treated with 500-μM pantothenate for 20 days. Control fibroblasts were treated with 500-μM Luperox (tert-butyl hydroperoxide) for 1 h as positive control of lipid peroxidation. Scale bar = 15 μm. $*p < 0.01$ between control and PKAN fibroblasts. $^{a}p < 0.01$ between untreated and treated fibroblasts. Data represent the mean ± SD of three separate experiments. A.U., arbitrary units

cellular iron uptake [44]. An alternative hypothesis supported by our results is that iron can be accumulated in the form of lipofuscin granules, which contain a high iron weight fraction (about 5%) and are markedly increased in PKAN cells.

Lipofuscin is a highly oxidized aggregate of covalently cross-linked proteins and lipids [45]. Metals, including Fe, Cu, Zn, Al, Mn, and Ca, comprise up to 2% of lipofuscin [46]. Lipofuscin is insoluble and not degradable by lysosomal enzymes or the proteasomal system, which is responsible for the recognition and degradation of misfolded and oxidatively damaged proteins [47]. These granules have been found in various cell types, including cardiomyocytes, hepatocytes,

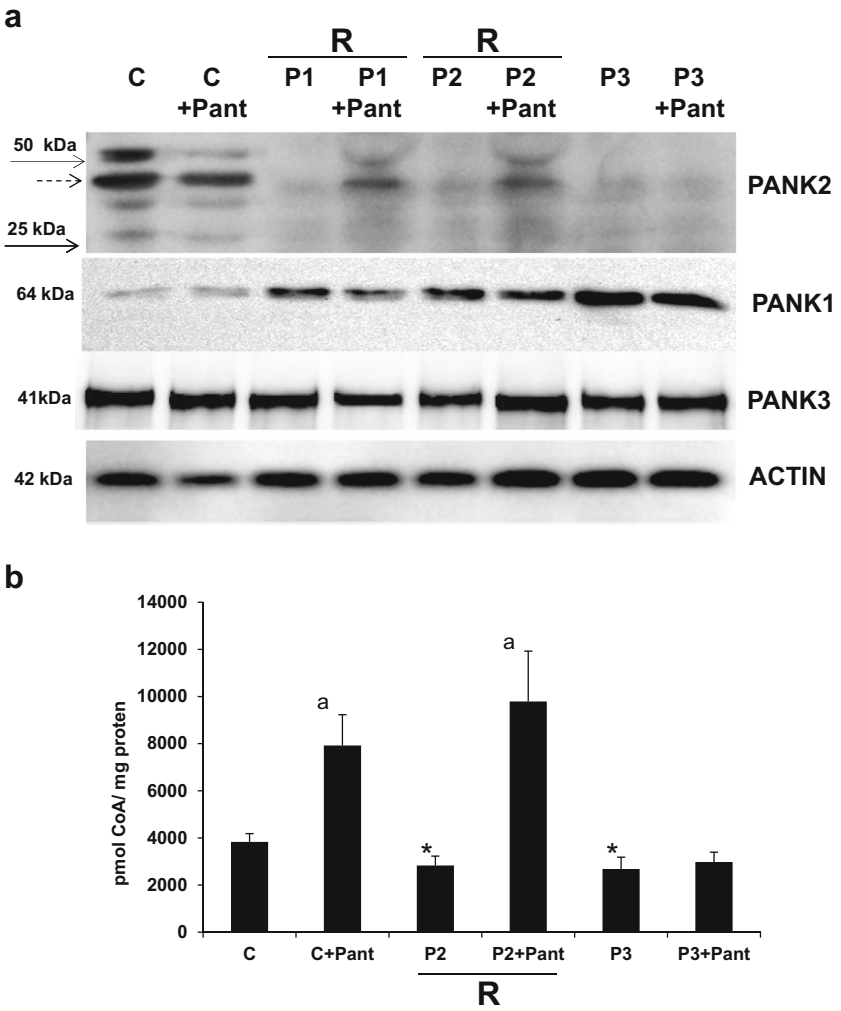

Fig. 8 Stabilization of PANK 2 and correction of CoA levels in responder patients. **a** Immunoblotting analysis of cellular extracts of control (C) cells and patients (P1, P2, and P3) fibroblasts. Control (C) and patient fibroblasts were treated with 500-μM pantothenate for 20 days. For control cells, data are a pool of three control cell lines. Fibroblast protein extracts (50 μg) were separated on a 12.5% SDS polyacrylamide gel and immunostained with antibodies against PANK1, PANK2, and PANK3. Dashed arrow points to PANK2 mature peptide of 48.5 kDa. Actin was used as a loading control. **b** Mitochondrial CoA levels of untreated and treated control and patient fibroblasts. CoA levels were determined by HPLC as is described in "Material and Methods." For control cells, the data are the mean ± SD for experiments conducted on three different control cell lines. Data represent the mean ± SD of three separate experiments. *$p < 0.01$ between control and PKAN fibroblats. [a]$p < 0.01$ between untreated and treated cells. R = pantothenate responder fibroblasts

and neurons, and are associated with cell senescence. One hypothesis predicts that mitochondria are involved in the formation of lipofuscin [48]. Thus, it has been demonstrated that isolated mitochondria can undergo transformation to lipofuscin granules without any additional factors [49]. The accumulation of lipofuscin is regarded as one of the best-known biomarkers of aging [50] and in our work, we demonstrated that this accumulation is associated with the presence of a typical senescent phenotype in PKAN cells. Several studies have proposed that lipofuscin actively participates in the pathophysiological alterations of senescent cells. Thus, it has been demonstrated that lipofuscin is able to inhibit the proteasome [51], the main cellular system for proteolytic degradation of damaged, modified, or misfolded proteins. Proteasomal inhibition is explained by its binding to exposed hydrophobic amino acid structures on the surface of lipofuscin [52]. Furthermore, lipofuscin it is able to reduce lysosomal function [53]. The combination of both factors, proteasome and lysosome inhibition, has been proposed to facilitate strongly the rate of lipofuscin formation [47].

In addition, one main factor of lipofuscin cytotoxicity is hypothesized to be its ability to incorporate transition metals, such as iron [46]. Binding of iron, as the most abundant transition metal in mammalian cells, results in a redox-active surface on lipofuscin, able to catalyze the Fenton reaction. This characteristic of lipofuscin may contribute to an increased level of radical formation and oxidatively modified cellular components, such as proteins, lipids, and nucleic acids, and

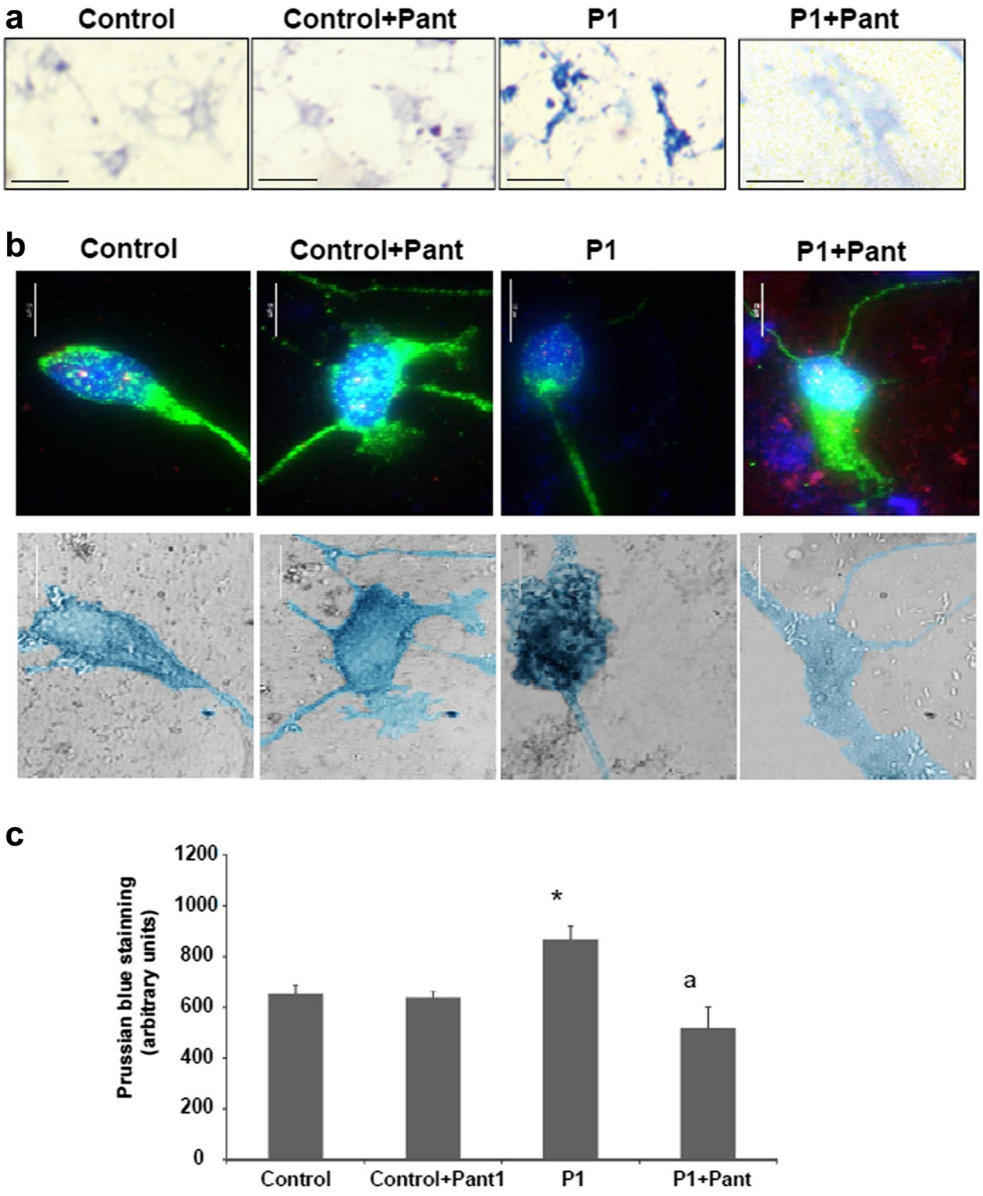

Fig. 9 PANK2 induced neurons show iron accumulation. **a** Bright-field pictures of Prussian Blue staining of control (C1) and P1 induced neurons after 500-μM pantothenate treatment during 10 days. Scale bar = 50 μm. **b** Representative merge fluorescence pictures at high magnification of control (C1) and P1 induced neurons immunostained with Tau (nuclei were revealed by Hoechst staining) and the corresponding bright-field pictures after Prussian Blue staining. Scale bar = 15 μm. **c** Quantification of Prussian Blue staining. Data represent the mean ± SD of three separate experiments (at least 50 neurons for each condition and experiment were examined). $^{*}p < 0.01$ between control and PKAN induced neurons. $^{a}p < 0.01$ between untreated and treated induced neurons. A.U., arbitrary units

eventually cell death [54]. The oxidative status has been previously analyzed in PKAN fibroblasts [14]. Sign of oxidative stress was detected in cells from patients, and ROS production was increased in these cells after exposure to iron. In agreement with these findings, we found increased amount of carbonylated proteins and mitochondrial lipid peroxidation in PANK2 mutant fibroblast, which were prevented by the treatment with pantothenate in responder mutant cells.

Non-specific systemic cytosolic abnormalities reported in cells from NBIA patients include bone marrow macrophages containing ceroid-lipofuscin and circulating lymphocytes with vacuoles and cytoplasmic inclusion bodies, similar to those seen in ceroid-lipofuscin storage disorders [31]. Lipofuscin accumulation in PKAN cells can result from lipid peroxidation, a process stimulated by iron [32, 33]. Abnormal accumulation of lipofuscin in NBIA has been also reported in conjunctival fibroblasts, retinal vessel pericytes, and macrophages [30]. These cytosolic abnormalities may shed some light on the underlying pathophysiology of NBIA in general and PKAN in particular.

Impaired iron metabolism in PKAN fibroblasts has been previously described [38], and it has been attributed to the impairment of mitochondrial ISC (iron-sulphur cluster) and heme biosynthesis pathways [14, 37]. In our work, we have clearly demonstrated that both processes are indeed impaired in PANK2 mutant fibroblasts. Additionally, pantothenate treatment partially corrected both alterations in responder cells. ISCs are prosthetic groups of many mitochondrial and cytosolic

enzymes, such as respiratory complexes and aconitases [55]. Therefore, ISC deficiency may affect many biosynthetic pathways and lead to mitochondrial dysfunction. One consequence of this deficiency is the inefficient utilization of iron that may cause iron accumulation in mitochondria. In turn, iron overload may cause increased free radical production that provokes further damage [56]. Furthermore, ineffective mitochondrial iron utilization may represent the signal that promotes the dysregulated iron import into the cells and, with time, leads to iron accumulation [37]. Thus, specific siRNA silencing of PANK2 in several human cell lines induced a mark reduction in cell proliferation together with unexpected signs of iron deficiency and increase of TfR1 expression levels [57]. As a consequence, the amount of aconitase, an iron-dependent enzyme, was also reduced, both in the cytosol and in the mitochondria. In agreement with these findings, our data supports the hypothesis that impaired mitochondrial iron metabolism produces cytosolic iron deficiency and a vicious cycle with increased iron uptake due to increased expression of Fe^{2+} transporters, such as DMT1 and subsequent deposition in mitochondria [58]. Interestingly, both alterations, reduced LIP and increased expression levels of DMT1, were partially restored by pantothenate treatment in responder fibroblasts.

PANK2 catalyzes the rate-limiting step in CoA biosynthesis and therefore, mutations in the gene encoding this enzyme have the potential to disrupt a number of essential metabolic processes by disrupting cellular CoA content [59]. As the CoA levels are dependent of both the supply of pantothenate and the level of expression of PANKs [60], an interesting treatment strategy would be to increase PANK2 expression levels in those patient cells with residual activity. Our results provide evidence that PANK2 expression levels can be stabilized by pantothenate treatment and can rescue all the pathological alterations including CoA levels, in selected patient cells with residual PANK2 expression. Pantothenate has no known toxicity in humans, and high oral doses of panthothenic acid or calcium pantothenate (up to 10 g per day for several weeks) do not appear to be toxic to humans. The efficacy of pantothenate supplementation in ameliorating symptoms in PKAN patients is currently unknown.

No definitive evidence is available showing decreased CoA content in human PANK2 deficient cells or tissues. Recently, the CoA levels in Pank2-KO mice were analyzed; no decrease was detected in any tissue in adult Pank2-KO mice [61]. The study suggests that the expression of the other PANK isoforms may compensate for the absence of PANK2 function. In our work, we show that despite a huge compensatory increase in PANK1 expression levels, CoA deficiency can be detected in mitochondria of PKAN fibroblasts and that pantothenate treatment induces a remarkable increase in CoA levels in responder cells.

Conclusion

Fibroblasts from PKAN patients show different patterns of PANK2 expression depending on the type of mutation. Mutant fibroblasts also show many of the pathological alterations associated with the disease, such as iron/lipofuscin accumulation, mitochondrial dysfunction, and oxidative stress.

Furthermore, we proved that pantothenate administration to PKAN cells with residual PANK2 expression prevented iron and lipofuscin accumulation, inhibited induced-cell death, restored bioenergetic alterations and oxidative stress, and partially rescued heme levels and respiratory activity.

The existence of residual enzyme activity in some affected individuals with PKAN raises the possibility of treatment using high dose pantothenate in selected patients.

Acknowledgements We thank María Pilar Burgos Domenech from IRNAS (Instituto de Recursos Naturales y Agrobiología de Sevilla) for her help with the ICP-MS assays and Carmen Jiménez de Haro from Instituto de Ciencia de Materiales de Sevilla (ICMS-US-CSIC) for her help with the SEM/EDX assays. We also thank Drs. Javier Abril Jaramillo, Anabel Vintimilla, Luis González Gutiérrez Solana, Pablo Mir, Marcos Madruga, Silvia Jesús, and Isidoro Caraballo for their support to the project.

Funding Information This work was supported by FIS PI16/00786 grant, Instituto de Salud Carlos III, Spain and Fondo Europeo de Desarrollo Regional (FEDER-Unión Europea), Proyectos de Investigación de Excelencia de la Junta de Andalucía CTS-5725 and BIO-122, DGICYT BFU2015-64536-R, and by AEPMI (Asociación de Enfermos de Patología Mitocondrial) and ENACH (Asociación de Enfermos de Neurodegeneración con Acumulación Cerebral de Hierro).

References

1. Gregory A, Polster BJ, Hayflick SJ (2009) Clinical and genetic delineation of neurodegeneration with brain iron accumulation. J Med Genet 46(2):73–80
2. Hayflick SJ, Westaway SK, Levinson B, Zhou B, Johnson MA, Ching KH, Gitschier J (2003) Genetic, clinical, and radiographic delineation of Hallervorden-Spatz syndrome. N Engl J Med 348(1): 33–40
3. Di Meo I, Tiranti V (2018) Classification and molecular pathogenesis of NBIA syndromes. Eur J Paediatr Neurol 22(2):272–284. https://doi.org/10.1016/j.ejpn.2018.01.008
4. Arber CE, Li A, Houlden H, Wray S (2016) Review: insights into molecular mechanisms of disease in neurodegeneration with brain iron accumulation: unifying theories. Neuropathol Appl Neurobiol 42(3):220–241. https://doi.org/10.1111/nan.12242
5. Levi S, Finazzi D (2014) Neurodegeneration with brain iron accumulation: update on pathogenic mechanisms. Front Pharmacol 5:99
6. Brunetti D, Dusi S, Morbin M, Uggetti A, Moda F, D'Amato I, Giordano C, d'Amati G et al (2012) Pantothenate kinase-associated neurodegeneration: altered mitochondria membrane potential and defective respiration in Pank2 knock-out mouse model. Hum Mol Genet 21(24):5294–5305. https://doi.org/10.1093/hmg/dds380
7. Gregory A, Hayflick SJ (2005) Neurodegeneration with brain iron accumulation. Folia Neuropathologica/Association of Polish

Neuropathologists and Medical Research Centre. Folia Neuropathol 43(4):286–296
8. Afshar K, Gonczy P, DiNardo S, Wasserman SA (2001) Fumble encodes a pantothenate kinase homolog required for proper mitosis and meiosis in *Drosophila melanogaster*. Genetics 157(3):1267–1276
9. Leonardi R, Zhang YM, Lykidis A, Rock CO, Jackowski S (2007) Localization and regulation of mouse pantothenate kinase 2. FEBS Lett 581(24):4639–4644
10. Kuo YM, Duncan JL, Westaway SK, Yang H, Nune G, Xu EY, Hayflick SJ, Gitschier J (2005) Deficiency of pantothenate kinase 2 (Pank2) in mice leads to retinal degeneration and azoospermia. Hum Mol Genet 14(1):49–57
11. Kuo YM, Hayflick SJ, Gitschier J (2007) Deprivation of pantothenic acid elicits a movement disorder and azoospermia in a mouse model of pantothenate kinase-associated neurodegeneration. J Inherit Metab Dis 30(3):310–317
12. Bosveld F, Rana A, van der Wouden PE, Lemstra W, Ritsema M, Kampinga HH, Sibon OC (2008) De novo CoA biosynthesis is required to maintain DNA integrity during development of the *Drosophila* nervous system. Hum Mol Genet 17(13):2058–2069
13. Rana A, Seinen E, Siudeja K, Muntendam R, Srinivasan B, van der Want JJ, Hayflick S, Reijngoud DJ et al (2010) Pantethine rescues a *Drosophila* model for pantothenate kinase-associated neurodegeneration. Proc Natl Acad Sci U S A 107(15):6988–6993
14. Campanella A, Privitera D, Guaraldo M, Rovelli E, Barzaghi C, Garavaglia B, Santambrogio P, Cozzi A et al (2012) Skin fibroblasts from pantothenate kinase-associated neurodegeneration patients show altered cellular oxidative status and have defective iron-handling properties. Hum Mol Genet 21(18):4049–4059. https://doi.org/10.1093/hmg/dds229
15. Adzhubei I, Jordan DM, Sunyaev SR (2013) Predicting functional effect of human missense mutations using PolyPhen-2. Current protocols in human genetics/editorial board, Jonathan L Haines [et al. Chapter 7:Unit7 20. https://doi.org/10.1002/0471142905.hg0720s76
16. Zhou B, Westaway SK, Levinson B, Johnson MA, Gitschier J, Hayflick SJ (2001) A novel pantothenate kinase gene (PANK2) is defective in Hallervorden-Spatz syndrome. Nat Genet 28(4):345–349
17. Dang TN, Bishop GM, Dringen R, Robinson SR (2010) The putative heme transporter HCP1 is expressed in cultured astrocytes and contributes to the uptake of hemin. Glia 58(1):55–65
18. Georgakopoulou EA, Tsimaratou K, Evangelou K, Fernandez Marcos PJ, Zoumpourlis V, Trougakos IP, Kletsas D, Bartek J et al (2013) Specific lipofuscin staining as a novel biomarker to detect replicative and stress-induced senescence. A method applicable in cryo-preserved and archival tissues. Aging 5(1):37–50
19. Boulton M, Marshall J (1985) Repigmentation of human retinal pigment epithelial cells in vitro. Exp Eye Res 41(2):209–218
20. Biesemeier A, Schraermeyer U, Eibl O (2011) Quantitative chemical analysis of ocular melanosomes in stained and non-stained tissues. Micron 42(5):461–470. https://doi.org/10.1016/j.micron.2011.01.004
21. Riemer J, Hoepken HH, Czerwinska H, Robinson SR, Dringen R (2004) Colorimetric ferrozine-based assay for the quantitation of iron in cultured cells. Anal Biochem 331(2):370–375. https://doi.org/10.1016/j.ab.2004.03.049
22. Tarohda T, Ishida Y, Kawai K, Yamamoto M, Amano R (2005) Regional distributions of manganese, iron, copper, and zinc in the brains of 6-hydroxydopamine-induced parkinsonian rats. Anal Bioanal Chem 383(2):224–234. https://doi.org/10.1007/s00216-005-3423-x
23. Shibata K, Nakai T, Fukuwatari T (2012) Simultaneous high-performance liquid chromatography determination of coenzyme A, dephospho-coenzyme A, and acetyl-coenzyme A in normal and pantothenic acid-deficient rats. Anal Biochem 430(2):151–155. https://doi.org/10.1016/j.ab.2012.08.010
24. Lowry OH, Rosebrough NJ, Farr AL, Randall RJ (1951) Protein measurement with the folin phenol reagent. J Biol Chem 193(1):265–275
25. Santambrogio P, Erba BG, Campanella A, Cozzi A, Causarano V, Cremonesi L, Galli A, Della Porta MG et al (2011) Over-expression of mitochondrial ferritin affects the JAK2/STAT5 pathway in K562 cells and causes mitochondrial iron accumulation. Haematologica 96(10):1424–1432. https://doi.org/10.3324/haematol.2011.042952
26. Rodriguez-Arribas M, Pizarro-Estrella E, Gomez-Sanchez R, Yakhine-Diop SM, Gragera-Hidalgo A, Cristo A, Bravo-San Pedro JM, Gonzalez-Polo RA et al (2016) IFDOTMETER: a new software application for automated immunofluorescence analysis. J Lab Autom 21(2):246–259. https://doi.org/10.1177/2211068215600650
27. Drouin-Ouellet J, Lau S, Brattas PL, Rylander Ottosson D, Pircs K, Grassi DA, Collins LM, Vuono R et al (2017) REST suppression mediates neural conversion of adult human fibroblasts via microRNA-dependent and -independent pathways. EMBO Mol Med 9(8):1117–1131. https://doi.org/10.15252/emmm.201607471
28. Shrigley S, Pircs K, Barker RA, Parmar M, Drouin-Ouellet J (2018) Simple generation of a high yield culture of induced neurons from human adult skin fibroblasts. J Vis Exp 132. https://doi.org/10.3791/56904
29. Zufferey R, Nagy D, Mandel RJ, Naldini L, Trono D (1997) Multiply attenuated lentiviral vector achieves efficient gene delivery in vivo. Nat Biotechnol 15(9):871–875. https://doi.org/10.1038/nbt0997-871
30. Luckenbach MW, Green WR, Miller NR, Moser HW, Clark AW, Tennekoon G (1983) Ocular clinicopathologic correlation of Hallervorden-Spatz syndrome with acanthocytosis and pigmentary retinopathy. Am J Ophthalmol 95(3):369–382
31. Swaiman KF, Smith SA, Trock GL, Siddiqui AR (1983) Sea-blue histiocytes, lymphocytic cytosomes, movement disorder and 59Fe-uptake in basal ganglia: Hallervorden-Spatz disease or ceroid storage disease with abnormal isotope scan? Neurology 33(3):301–305
32. Defendini R, Markesbery WR, Mastri AR, Duffy PE (1973) Hallervorden-Spatz disease and infantile neuroaxonal dystrophy. Ultrastructural observations, anatomical pathology and nosology. J Neurol Sci 20(1):7–23
33. Park BE, Netsky MG, Betsill WL Jr (1975) Pathogenesis of pigment and spheroid formation in Hallervorden-Spatz syndrome and related disorders. Neurology 25(12):1172–1178
34. Bindewald-Wittich A, Han M, Schmitz-Valckenberg S, Snyder SR, Giese G, Bille JF, Holz FG (2006) Two-photon-excited fluorescence imaging of human RPE cells with a femtosecond Ti:sapphire laser. Invest Ophthalmol Vis Sci 47(10):4553–4557. https://doi.org/10.1167/iovs.05-1562
35. Newbury DE, Ritchie NW (2015) Performing elemental microanalysis with high accuracy and high precision by scanning electron microscopy/silicon drift detector energy-dispersive X-ray spectrometry (SEM/SDD-EDS). J Mater Sci 50(2):493–518. https://doi.org/10.1007/s10853-014-8685-2
36. Shioji K, Oyama Y, Okuma K, Nakagawa H (2010) Synthesis and properties of fluorescence probe for detection of peroxides in mitochondria. Bioorg Med Chem Lett 20(13):3911–3915. https://doi.org/10.1016/j.bmcl.2010.05.017
37. Orellana DI, Santambrogio P, Rubio A, Yekhlef L, Cancellieri C, Dusi S, Giannelli SG, Venco P et al (2016) Coenzyme A corrects pathological defects in human neurons of PANK2-associated neurodegeneration. EMBO Mol Med 8(10):1197–1211. https://doi.org/10.15252/emmm.201606391
38. Santambrogio P, Dusi S, Guaraldo M, Rotundo LI, Broccoli V, Garavaglia B, Tiranti V, Levi S (2015) Mitochondrial iron and energetic dysfunction distinguish fibroblasts and induced neurons

from pantothenate kinase-associated neurodegeneration patients. Neurobiol Dis 81:144–153. https://doi.org/10.1016/j.nbd.2015.02.030

39. Ingrassia R, Memo M, Garavaglia B (2017) Ferrous iron up-regulation in fibroblasts of patients with beta propeller protein-associated neurodegeneration (BPAN). Front Genet 8:18. https://doi.org/10.3389/fgene.2017.00018
40. Nunez MT, Urrutia P, Mena N, Aguirre P, Tapia V, Salazar J (2012) Iron toxicity in neurodegeneration. Biometals 25(4):761–776. https://doi.org/10.1007/s10534-012-9523-0
41. Lan AP, Chen J, Chai ZF, Hu Y (2016) The neurotoxicity of iron, copper and cobalt in Parkinson's disease through ROS-mediated mechanisms. Biometals 29(4):665–678. https://doi.org/10.1007/s10534-016-9942-4
42. Salvador GA, Uranga RM, Giusto NM (2010) Iron and mechanisms of neurotoxicity. Int J Alzheimers Dis 2011:720658–720659. https://doi.org/10.4061/2011/720658
43. Kruer MC (2013) The neuropathology of neurodegeneration with brain iron accumulation. Int Rev Neurobiol 110:165–194. https://doi.org/10.1016/B978-0-12-410502-7.00009-0
44. Matsunaga T, Kotamraju S, Kalivendi SV, Dhanasekaran A, Joseph J, Kalyanaraman B (2004) Ceramide-induced intracellular oxidant formation, iron signaling, and apoptosis in endothelial cells: protective role of endogenous nitric oxide. J Biol Chem 279(27):28614–28624. https://doi.org/10.1074/jbc.M400977200
45. Double KL, Dedov VN, Fedorow H, Kettle E, Halliday GM, Garner B, Brunk UT (2008) The comparative biology of neuromelanin and lipofuscin in the human brain. Cell Mol Life Sci 65(11):1669–1682. https://doi.org/10.1007/s00018-008-7581-9
46. Jolly RD, Douglas BV, Davey PM, Roiri JE (1995) Lipofuscin in bovine muscle and brain: a model for studying age pigment. Gerontology 41(Suppl 2):283–295
47. Jung T, Bader N, Grune T (2007) Lipofuscin: formation, distribution, and metabolic consequences. Ann N Y Acad Sci 1119:97–111. https://doi.org/10.1196/annals.1404.008
48. Konig J, Ott C, Hugo M, Jung T, Bulteau AL, Grune T, Hohn A (2017) Mitochondrial contribution to lipofuscin formation. Redox Biol 11:673–681. https://doi.org/10.1016/j.redox.2017.01.017
49. Frolova MS, Surin AM, Braslavski AV, Vekshin NL (2015) Degradation of mitochondria to lipofuscin upon heating and illumination. Biofizika 60(6):1125–1131
50. Brunk UT, Terman A (2002) Lipofuscin: mechanisms of age-related accumulation and influence on cell function. Free Radic Biol Med 33(5):611–619
51. Powell SR, Wang P, Divald A, Teichberg S, Haridas V, McCloskey TW, Davies KJ, Katzeff H (2005) Aggregates of oxidized proteins (lipofuscin) induce apoptosis through proteasome inhibition and dysregulation of proapoptotic proteins. Free Radic Biol Med 38(8):1093–1101. https://doi.org/10.1016/j.freeradbiomed.2005.01.003
52. Hohn A, Grune T (2013) Lipofuscin: formation, effects and role of macroautophagy. Redox Biol 1:140–144. https://doi.org/10.1016/j.redox.2013.01.006
53. Kurz T, Terman A, Gustafsson B, Brunk UT (2008) Lysosomes and oxidative stress in aging and apoptosis. Biochim Biophys Acta 1780(11):1291–1303. https://doi.org/10.1016/j.bbagen.2008.01.009
54. Reeg S, Grune T (2015) Protein oxidation in aging: does it play a role in aging progression? Antioxid Redox Signal 23(3):239–255. https://doi.org/10.1089/ars.2014.6062
55. Lill R, Srinivasan V, Muhlenhoff U (2014) The role of mitochondria in cytosolic-nuclear iron-sulfur protein biogenesis and in cellular iron regulation. Curr Opin Microbiol 22:111–119. https://doi.org/10.1016/j.mib.2014.09.015
56. Lu C, Cortopassi G (2007) Frataxin knockdown causes loss of cytoplasmic iron-sulfur cluster functions, redox alterations and induction of heme transcripts. Arch Biochem Biophys 457(1):111–122. https://doi.org/10.1016/j.abb.2006.09.010
57. Poli M, Derosas M, Luscieti S, Cavadini P, Campanella A, Verardi R, Finazzi D, Arosio P. Pantothenate kinase-2 (Pank2) silencing causes cell growth reduction, cell-specific ferroportin upregulation and iron deregulation. Neurobiol Dis. 2010 Aug 39(2):204–10. https://doi.org/10.1016/j.nbd.2010.04.009. Epub 2010 Apr 23
58. Huang ML, Lane DJ, Richardson DR (2011) Mitochondrial mayhem: the mitochondrion as a modulator of iron metabolism and its role in disease. Antioxid Redox Signal 15(12):3003–3019. https://doi.org/10.1089/ars.2011.3921
59. Leonardi R, Zhang YM, Rock CO, Jackowski S (2005) Coenzyme A: back in action. Prog Lipid Res 44(2–3):125–153. https://doi.org/10.1016/j.plipres.2005.04.001
60. Leonardi R, Jackowski S (2007) Biosynthesis of pantothenic acid and coenzyme A. EcoSal Plus 2(2). https://doi.org/10.1128/ecosalplus.3.6.3.4
61. Garcia M, Leonardi R, Zhang YM, Rehg JE, Jackowski S (2012) Germline deletion of pantothenate kinases 1 and 2 reveals the key roles for CoA in postnatal metabolism. PLoS One 7(7):e40871. https://doi.org/10.1371/journal.pone.0040871